A multiple scattering formulation to design meta-trenches for mitigating low-frequency ground-borne vibrations induced by surface railways and subways

A multiple scattering formulation to design meta-trenches for mitigating low-frequency ground-borne vibrations induced by surface railways and subways

Kemeng Cui[a,b], Zhao-Dong Xu[a,*], Alessandro Marzani[b], Xingbo Pu[b,c,*]

[a] *China-Pakistan Belt and Road Joint Laboratory on Smart Disaster Prevention of Major Infrastructures, School of Civil Engineering, Southeast University, 211189, Nanjing, China*
[b] *Department of Civil, Chemical, Environmental and Materials Engineering, University of Bologna, 40136 Bologna, Italy*
[c] *Department of Mechanical and Aerospace Engineering, The Hong Kong University of Science and Technology, Clear Water Bay, Kowloon, Hong Kong*

Abstract

We propose a multiple scattering formulation to investigate the performance of *meta-trenches*. The meta-trench is a novel device, composed of an array of resonant units buried in the ground in a proper arrangement, aimed at reducing the railway and/or subway induced ground motion by exploiting its scattering and resonant properties. Compared to classical open trenches the contribution of resonators is to improve the wave mitigation performance of the trench in the low-frequency regime.

The proposed formulation allows to consider the wave source anywhere in the half-space and a generic distribution of resonators in terms of number and position. The incident wave field generated by the source, train or subway, along with the scattered wave fields produced by the resonant units that make up the meta-trench, are modeled via Green's functions. The multiple scattering formulation enables the solution of coupled wave problems by determining the amplitudes of scattered wave fields at various frequencies. By comparing with finite element simulations, we demonstrate that in both buried source (i.e., subway) and surface-located source (i.e., ground railway) scenarios, our analytical formulation is able to properly model the dynamics of the coupled problems with a noticeable computational cost saving. Opening to fast and reliable parametric simulations, our formulation allows for a deeper knowledge of the wave interaction processes, resulting thus in a reliable tool for predicting the coupled wave field under both bulk and Rayleigh waves.

Keywords: elastic metamaterials, meta-trench, buried-source problem, railway/subway induced vibrations, elastic waves

1. Introduction

Ground railway or subway induced vibrations are one of the major source of annoyance for the built environment and a matter of growing concern, especially in dense urbanized area. These vibrations in the form of mechanical waves propagate through the soil into adjacent buildings interfering with the daily life of residents, causing damages and preventing the usage of sensitive equipment [1, 2]. Therefore, reducing railway and/or subway induced vibrations to protect adjacent structures is an urgent matter.

To this goal, a common approach in practical engineering is to impede the waves to propagate from the source to the protected structures by placing barriers, like open or in-filled trenches [3–6] or rows of piles [7–10]. These barriers, by exploiting geometric scattering, effectively attenuate the wave energy induced by railways and

*Corresponding authors
Email addresses: zhdxu@163.com (Zhao-Dong Xu), mexingbop@ust.hk (Xingbo Pu)

subways at the target. However, they barely contribute to the low-frequency regime where the wavelengths are quite long unless they are characterized by unrealistic geometrical dimensions. As low-frequency waves are more harmful to buildings and they travel much farther due to their smaller attenuation compared to high-frequency waves, more attention to them is needed.

Recently, the advent of resonant elastic metamaterials has provided unprecedented ways to face such dilemma [11, 12]. In particular, metasurfaces, artificial planar metamaterials composed of sub-wavelength resonators, have shown outstanding performance in manipulating wave propagation. The applications range from wave localization [13–15] energy harvesting [16, 17] to vibration mitigation [18–20]. By the use of resonators, waves in specific frequency bands can be guided away from the target object to protect it [21–23]. For instance, many works have shown how surface elastic waves propagating in a half-space can be converted into bulk waves with the aid of sub-wavelength resonators placed atop the soil, namely metasurfaces [24–26]. While appealing, metasurfaces with resonators distributed at the soil surface need a large area limiting thus their engineering feasibility especially in densely urbanized areas [27–29].

This limitation has motivated the study of a novel solution for the mitigation of railway/subway induced vibrations, the so-called meta-trench (see in Fig. 1), where the resonant elements are distributed into a classic trench avoiding thus the need of spreading them over a large surface area. The idea is that by tuning resonance frequencies of resonators, the metatrench should interact with low-frequency waves and eventually mitigate their effect.

While the dynamics of a metasurface can be predicted by its dispersion relation [30–34], which carries information on bandgaps, waves attenuation, cut-on and cut-off frequencies, the dynamics of the meta-trench can be unveiled only by the full wave-field which is generally computed by numerical schemes like finite elements (FE). Still, FE simulations suffer the computational cost related to large-scale models needed to predict the far field, which in turn limits the possibility of extensive simulations for a parametric design of the meta-trench.

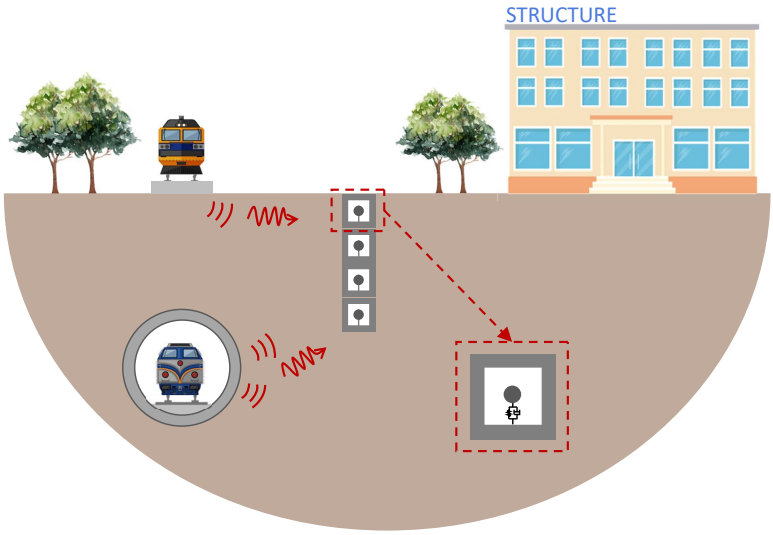

Fig. 1. Schematic of finite elastic metamaterials in mitigating railway-induced vibration.

In light of this, we propose here an efficient analytical multiple scattering formulation to model the interaction of incident waves with the meta-trench. The proposed formulation extends a recent scheme [35–37] where both the wave source and the resonators were constrained atop the elastic half-space. Here, we removed such constraints allowing the formulation to model also subways induced vibrations and meta-trenches. In particular,

we first formulate the Green's functions for a buried-source problem to model both the incident wave field generated by an inner source and the scattered wave fields of the buried resonators. While the amplitude of the inner source is given in input to the problem, the amplitudes of the scattered fields are unknown and coupled to each other. The proposed multiple scattering formulation, where the total wave field is formed by the incident and scattered wave fields, allows us to find such unknowns and thus to obtain the true coupled wave field.

The formulation offers a computationally effective tool for analyzing the coupled interaction of waves and resonant metamaterials generically distributed in a bi-dimensional setting. Particularly, it allows to study and design finite-size meta-trenches, enriching thus the engineering application scenarios devoted to waves mitigation.

This paper is organized as follows. In Section 2, we briefly describe the problem statement. In Section 3, we develop a multiple scattering formulation to model the coupled interaction between an array of resonators distributed in a bi-dimensional half-space. Then we apply the formulation to model a meta-trench aimed at mitigating railway and subway induced vibrations and validate the results with numerical FE simulations in Section 4. Finally, we summarize the main conclusions of our work in Section 5.

2. Statement of the problem

We consider an array of N mechanical resonators embedded in a two-dimensional (2D) isotropic, linear elastic half-space in plane-strain $x-z$ condition (see Fig. 2). Given the significance of the vertical component in train-induced ground vibrations [2, 38], for the sake of simplicity we limit our focus solely on the single-degree-of-freedom (SDOF) resonator in this study (see the two degrees of freedom model in Appendix D). Each resonator, placed at position (x_{rn}, z_{rn}), with $n = 1, 2, ..., N$, is modeled as a vertical mass-spring-dashpot system with mass m_n, stiffness k_n, and viscous damping coefficient c_n, placed on a foundation of width b. A harmonic source $Q_z e^{i\omega t}$, applied to an arbitrary location (x_0, z_0) and acting over a footprint area of width a (see Fig. 2), excites the so-called incident wavefield with displacement components $u_0(x, z)$ and $w_0(x, z)$ along the x and z directions, respectively. The nth resonator, oscillating due to an imposed vertical base motion at frequency ω, generates an additional scattered wavefield with displacements components $u_n(x, z)$ and $w_n(x, z)$ proportional to the force exchanged with the soil. Such force has a magnitude $Q_n = Z_n w(x_{rn}, z_{rn})$ where Z_n is the resonator impedance known for a given ω, while $w(x_{rn}, z_{rn})$ is the overall vertical displacement at the resonator base due to the given incident and the N unknown coupled scattered wave fields. The $w(x_{rn}, z_{rn})$ value for each resonator is indeed the output of the multiple scatting formulation. As such, by expressing the total wavefield at a generic location (x, z) as:

$$u(x, z) = u_0(x, z) + \sum_{n=1}^{N} u_n(x, z) \tag{1a}$$

$$w(x, z) = w_0(x, z) + \sum_{n=1}^{N} w_n(x, z) \tag{1b}$$

where the subscript 0 denotes the incident wave field and the subscript n denotes the scattered wave field of the nth resonator, the proposed formulation aims at findings the u_n and w_n values.

In previous works [35–37], where both the force and the resonators were restricted atop the soil surface, namely $h_0 = 0$ and $h_n = 0$ for $n = 1, 2, ..., N$, see Fig. 2, the Green's functions of the Lamb's problem were

adopted to set the multiple scattering formulation. Following the same procedure, we first derive the Green's functions for the buried-source problem, and then develop an analytical formulation for a half-space excited by a harmonic buried source coupled with an array of arbitrarily distributed resonators.

In particular, as we focus our interest on the interaction between half-space and resonators at low frequencies, the geometric scattering due to the trench is neglected as the wavelengths are much larger than the dimension of resonators.

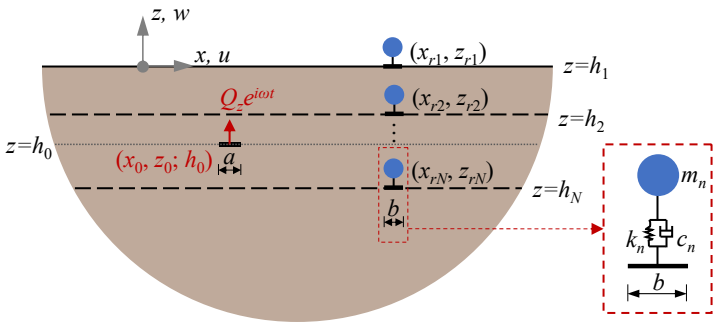

Fig. 2. Schematic of finite arbitrarily distributed resonators in an elastic half-space.

3. Formulation

3.1. The Green's function of the buried-source problem

Let us consider a buried excitation force with amplitude Q_z. In the following derivation we restrict our discussions to a time-harmonic regime so that the term $e^{i\omega t}$ is omitted to ease the notation. The source is applied at (x_0, z_0) in a 2D half space at a depth equal to h (non-positive value) from the free surface, as shown in Fig. 3.

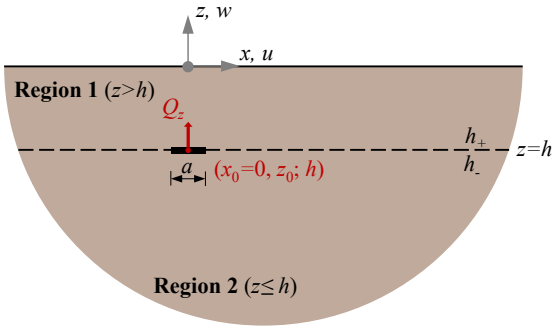

Fig. 3. Schematic of the buried-source problem.

The 2D wave equation in displacement potentials reads:

$$\nabla^2\Phi + k_p^2\Phi = 0, \quad \nabla^2\Psi_y + k_s^2\Psi_y = 0, \quad -\infty < x < \infty, z \leq 0. \tag{2}$$

where $\Phi(x,z)$ and $\Psi_y(x,z)$ denote the wave dilatational potential and distorsional potential, respectively; $k_p = \omega/c_p$ and $k_s = \omega/c_s$ are the compressional and shear wave numbers in the half-space, respectively, in which $c_p = \sqrt{(\lambda' + 2\mu')/\rho}$ and $c_s = \sqrt{\mu'/\rho}$ are the compressional and shear wave velocities; whereas $\lambda' = \lambda(1 + 2\xi i)$ and $\mu' = \mu(1 + 2\xi i)$ are the Lamé constants being ξ and ρ the hysteretic damping ratio and mass density of the half-space.

Fourier transforming along x direction Eqs. (2) lead to two ordinary differential equations:

$$\frac{\mathrm{d}^2\bar{\Phi}}{\mathrm{d}z^2} - (k^2 - k_p^2)\bar{\Phi} = 0, \quad \frac{\mathrm{d}^2\bar{\Psi}_y}{\mathrm{d}z^2} - (k^2 - k_s^2)\bar{\Psi}_y = 0, \tag{3}$$

in which k denotes the wave number. The general solutions of Eqs. (3) have the form:

$$\bar{\Phi} = A_1\mathrm{e}^{pz} + A_2\mathrm{e}^{-pz}, \quad \bar{\Psi}_y = B_1\mathrm{e}^{qz} + B_2\mathrm{e}^{-qz}, \tag{4}$$

with:

$$p^2 = k^2 - k_p^2, \quad q^2 = k^2 - k_s^2, \tag{5}$$

and where A_1, A_2, B_1, B_2 are unknown coefficients to be determined from boundary conditions. A convenient mathematical treatment for this type of problem [39] is to divide the half-space into two regions one with $0 \geq z > h$ (Region 1 in Fig. 3) and the other one with $z \leq h$ (Region 2 in Fig. 3). We reorganize the solutions of the wave equations as:

$$\bar{\Phi} = \begin{cases} A_{L1}\mathrm{e}^{pz} + A_{L2}\mathrm{e}^{-pz}, & 0 \geq z > h \\ A_{H1}\mathrm{e}^{pz} + A_{H2}\mathrm{e}^{-pz}, & z \leq h \end{cases} \tag{6a}$$

$$\bar{\Psi}_y = \begin{cases} B_{L1}\mathrm{e}^{qz} + B_{L2}\mathrm{e}^{-qz}, & 0 \geq z > h \\ B_{H1}\mathrm{e}^{qz} + B_{H2}\mathrm{e}^{-qz}, & z \leq h \end{cases} \tag{6b}$$

in which the subscripts L and H denote coefficients for Region 1 and Region 2, respectively.

Imposing traction-free boundary conditions at the free surface ($z = 0$), and enforcing the continuity of stresses and displacements at regions interface ($z = h$), yields in the Fourier domain to the following three sets of equations:

$$\bar{\sigma}_z(k, 0) = 0, \quad \bar{\tau}_{zx}(k, 0) = 0 \tag{7a}$$

$$\bar{\sigma}_z(k, h_-) - \bar{\sigma}_z(x, h_+) = \begin{cases} \frac{2Q_z}{ka}\sin\frac{ka}{2}, & |x| < a \\ 0, & \text{elsewhere} \end{cases}, \quad \bar{\tau}_{zx}(k, h_-) - \bar{\tau}_{zx}(k, h_+) = 0 \tag{7b}$$

$$\bar{u}(k, h_-) = \bar{u}(k, h_+), \quad \bar{w}(k, h_-) = \bar{w}(k, h_+) \tag{7c}$$

in which h_+ and h_- denote the top and bottom edges of the interface $z = h$ (see Fig. 3).

According to the Helmholtz decomposition, the Fourier transformed displacement components take the form:

$$\bar{u}(k, z) = \begin{cases} \mathrm{i}k(A_{L1}\mathrm{e}^{pz} + A_{L2}\mathrm{e}^{-pz}) - q(B_{L1}\mathrm{e}^{qz} - B_{L2}\mathrm{e}^{-qz}), & 0 \geq z > h \\ \mathrm{i}k(A_{H1}\mathrm{e}^{pz} + A_{H2}\mathrm{e}^{-pz}) - q(B_{H1}\mathrm{e}^{qz} - B_{H2}\mathrm{e}^{-qz}), & z \leq h \end{cases} \tag{8a}$$

$$\bar{w}(k, z) = \begin{cases} p(A_{L1}\mathrm{e}^{pz} - A_{L2}\mathrm{e}^{-pz}) + \mathrm{i}k(B_{L1}\mathrm{e}^{qz} + B_{L2}\mathrm{e}^{-qz}), & 0 \geq z > h \\ p(A_{H1}\mathrm{e}^{pz} - A_{H2}\mathrm{e}^{-pz}) + \mathrm{i}k(B_{H1}\mathrm{e}^{qz} + B_{H2}\mathrm{e}^{-qz}), & z \leq h \end{cases} \tag{8b}$$

where A_{H2} and B_{H2} must be null to avoid an unbounded solution at $z = -\infty$. With the aid of Hooke's law the stress components can be expressed as:

$$\bar{\sigma}_z(k, z) = \begin{cases} -\mu({k_s}^2 - 2k^2)(A_{L1}\mathrm{e}^{pz} + A_{L2}\mathrm{e}^{-pz}) + 2\mu\mathrm{i}kq(B_{L1}\mathrm{e}^{qz} + B_{L2}\mathrm{e}^{-qz}), & 0 \geq z > h \\ -\mu({k_s}^2 - 2k^2)(A_{H1}\mathrm{e}^{pz} + A_{H2}\mathrm{e}^{-pz}) + 2\mu\mathrm{i}kq(B_{H1}\mathrm{e}^{qz} + B_{H2}\mathrm{e}^{-qz}), & z \leq h \end{cases} \tag{9a}$$

$$\bar{\tau}_{zx}(k,z) = \begin{cases} 2\mu ikp(A_{L1}\mathrm{e}^{pz} - A_{L2}\mathrm{e}^{-pz}) + \mu({k_s}^2 - 2k^2)(B_{L1}\mathrm{e}^{qz} + B_{L2}\mathrm{e}^{-qz}), & 0 \geq z > h \\ 2\mu ikp(A_{H1}\mathrm{e}^{pz} - A_{H2}\mathrm{e}^{-pz}) + \mu({k_s}^2 - 2k^2)(B_{H1}\mathrm{e}^{qz} + B_{H2}\mathrm{e}^{-qz}), & z \leq h \end{cases} \tag{9b}$$

where μ is the shear modulus of the half-space. Combing Eqs. (7-9) yields for the coefficients:

$$A_{L1} = \frac{Q_z}{\mu a \gamma_1 {k_s}^2} \cdot \frac{(\mathrm{e}^{hp}\gamma_2 + 4\mathrm{e}^{hq}k^2\beta)}{k} \cdot \sin\frac{ka}{2} \tag{10a}$$

$$A_{L2} = \frac{Q_z}{\mu a \gamma_1 {k_s}^2} \cdot \frac{\mathrm{e}^{hp}\gamma_1}{k} \cdot \sin\frac{ka}{2} \tag{10b}$$

$$B_{L1} = \frac{Q_z}{\mu a \gamma_1 {k_s}^2} \cdot \frac{-(4\mathrm{e}^{hp}pq\beta + \mathrm{e}^{hp}\gamma_2)\mathrm{i}}{q} \cdot \sin\frac{ka}{2} \tag{10c}$$

$$B_{L2} = \frac{Q_z}{\mu a \gamma_1 {k_s}^2} \cdot \frac{-\mathrm{e}^{hq}\gamma_1\mathrm{i}}{q} \cdot \sin\frac{ka}{2} \tag{10d}$$

$$A_{H1} = \frac{Q_z}{\mu a \gamma_1 {k_s}^2} \cdot \frac{(\mathrm{e}^{hp}\gamma_2 - \mathrm{e}^{-hp}\gamma_1 + 4\mathrm{e}^{hq}k^2\beta)}{k} \cdot \sin\frac{ka}{2} \tag{10e}$$

$$B_{H1} = \frac{Q_z}{\mu a \gamma_1 {k_s}^2} \cdot \frac{-(4\mathrm{e}^{hp}pq\beta + \mathrm{e}^{hq}\gamma_2 + \mathrm{e}^{-hq}\gamma_1)\mathrm{i}}{q} \cdot \sin\frac{ka}{2} \tag{10f}$$

with $\beta = {k_s}^2 - 2k^2$, $\gamma_1 = 4k^2pq - \beta^2$ and $\gamma_2 = 4k^2pq + \beta^2$.

By substituting Eqs. (10) into Eqs. (8) and performing the inverse Fourier transform, we obtain the sought Green's functions:

$$\mathbf{G}(x,z;h) = \frac{1}{2\pi\mu a}\int_{-\infty}^{\infty} \frac{1}{{k_s}^2\gamma_1}\mathbf{\Delta}\mathbf{Y}\sin\frac{ka}{2}\mathrm{e}^{\mathrm{i}kx}\,\mathrm{d}k, \tag{11}$$

where $\mathbf{G}(x,z;h) = [G_{uz}, G_{wz}]^T$, $\mathbf{Y} = [\mathrm{e}^{pz}, \mathrm{e}^{-pz}, \mathrm{e}^{qz}, \mathrm{e}^{-qz}]^T$, and $\mathbf{\Delta}$ is equal to:

$$\mathbf{\Delta} = \begin{bmatrix} \mathrm{i}(\mathrm{e}^{hp}\gamma_2 + 4\mathrm{e}^{hq}k^2\beta) & \mathrm{i}\mathrm{e}^{hp}\gamma_1 & \mathrm{i}(\mathrm{e}^{hq}\gamma_2 + 4\mathrm{e}^{hp}pq\beta) & -\mathrm{i}\mathrm{e}^{hq}\gamma_1 \\ \frac{p}{k}(\mathrm{e}^{hp}\gamma_2 + 4\mathrm{e}^{hq}k^2\beta) & -\frac{p}{k}\mathrm{e}^{hp}\gamma_1 & \frac{k}{q}(\mathrm{e}^{hq}\gamma_2 + 4\mathrm{e}^{hp}pq\beta) & \frac{k}{q}\mathrm{e}^{hq}\gamma_1 \end{bmatrix}, \tag{12}$$

if $z > h$ and equals to:

$$\mathbf{\Delta} = \begin{bmatrix} \mathrm{i}(\mathrm{e}^{hp}\gamma_2 - \mathrm{e}^{-hp}\gamma_1 + 4\mathrm{e}^{hq}k^2\beta) & 0 & \mathrm{i}(\mathrm{e}^{hq}\gamma_2 + \mathrm{e}^{-hq}\gamma_1 + 4\mathrm{e}^{hp}pq\beta) & 0 \\ \frac{p}{k}(\mathrm{e}^{hp}\gamma_2 - \mathrm{e}^{-hp}\gamma_1 + 4\mathrm{e}^{hq}k^2\beta) & 0 & \frac{k}{q}(\mathrm{e}^{hq}\gamma_2 + \mathrm{e}^{-hq}\gamma_1 + 4\mathrm{e}^{hp}pq\beta) & 0 \end{bmatrix}, \tag{13}$$

if $z \leq h$.

To ensure the numerical stability in the computation of the Green's function, a small hysteretic damping ratio of $\xi = 1\%$ is introduced in the substrate.

3.2. Multiple scattering formulation

Considering the Green's functions related to a buried source or to source placed atop the half-space [35], we can obtain the total wave field. Let us first consider the incident wave field:

$$u_0(x,z) = Q_z G_{0uz}(x - x_0, z_0; h_0), \tag{14a}$$

$$w_0(x,z) = Q_z G_{0wz}(x - x_0, z_0; h_0), \tag{14b}$$

where for a buried source scenario the Green's functions take form of Eqs. (11), whereas if the source is located

at the soil surface $h_0 = 0$ the Green's functions degenerate to the form:

$$G_{0uz} = \frac{1}{\pi\mu a}\int_{-\infty}^{\infty}[\frac{\mathrm{i}({k_s}^2 - 2k^2)\mathrm{e}^{pz} + 2\mathrm{i}pq\mathrm{e}^{qz}}{4k^2pq - ({k_s}^2 - 2k^2)^2}\cdot\sin\frac{ka}{2}]\mathrm{e}^{\mathrm{i}k(x-x_0)}\,\mathrm{d}k, \tag{15a}$$

$$G_{0wz} = \frac{1}{\pi\mu a}\int_{-\infty}^{\infty}[\frac{({k_s}^2 - 2k^2)p\mathrm{e}^{pz} + 2k^2p\mathrm{e}^{qz}}{4k^2pq - ({k_s}^2 - 2k^2)^2}\cdot\frac{1}{k}\cdot\sin\frac{ka}{2}]\mathrm{e}^{\mathrm{i}k(x-x_0)}\,\mathrm{d}k, \tag{15b}$$

Now, let us move to the scattered wave field. The force amplitude $Q_n = Z_n w(x_{rn}, z_{rn})$ of the nth resonator is obtained from the dynamic equilibrium equation for a harmonic base motion $w(x_n, z_n)$ as:

$$Q_n = Z_n w(x_{rn}, z_{rn}) = \frac{m_n\omega^2(\mathrm{i}\omega c_n + m_n{\omega_{rn}}^2)}{-m_n\omega^2 + \mathrm{i}\omega c_n + m_n{\omega_{rn}}^2}w(x_{rn}, z_{rn}) \quad n = 1, ..., N, \tag{16}$$

where $\omega_{rn} = 2\pi f_{rn} = \sqrt{k_n/m_n}$.

We can rewrite the total wavefield in Eqs. (1) as:

$$u(x,z) = u_0(x,z) + \sum_{n=1}^{N} Q_n G_{uz}(x - x_{rn}, z; h_{rn}) \tag{17a}$$

$$w(x,z) = w_0(x,z) + \sum_{n=1}^{N} Q_n G_{wz}(x - x_{rn}, z; h_{rn}) \tag{17b}$$

Once the force Q_n is obtained, the total wavefield can be computed via Eqs. (17a) and (17b). As Q_n is related to w, as it can be seen from Eq. (16), it can be computed substituting Eq. (17b) only into Eq. (16). We specify this at all resonator locations (x_{rj}, z_{rj}) which leads to:

$$Z_j^{-1}Q_j = w_0(x_{rj}, z_{rj}) + \sum_{n=1}^{N} Q_n G_{wz}(x_{rj} - x_{rn}, z_{rj}; h_{rn}), \tag{18}$$

After some algebra, Eq. (18) can be rearranged in a matrix form as:

$$\mathbf{Q} = \mathbf{A}^{-1}\mathbf{W_0} \tag{19}$$

where $\mathbf{Q} = [Q_1, Q_2, \cdots, Q_N]^T$ is the vector collecting the sought resonator force amplitudes, whereas:

$$\mathbf{A} = \begin{bmatrix} Z_1^{-1} - G_{wz}(0, z_{r1}; h_1) & -G_{wz}(x_{r1} - x_{r2}, z_{r1}; h_2) & \cdots & -G_{wz}(x_{r1} - x_{rN}, z_{r1}; h_N) \\ -G_{wz}(x_{r2} - x_{r1}, z_{r2}; h_1) & Z_2^{-1} - G_{wz}(0, z_{r2}; h_2) & \cdots & -G_{wz}(x_{r2} - x_{rN}, z_{r2}; h_N) \\ \vdots & \vdots & \ddots & \vdots \\ -G_{wz}(x_{rN} - x_{r1}, z_{rN}; h_1) & -G_{wz}(x_{rN} - x_{r2}, z_{rN}; h_2) & \cdots & Z_N^{-1} - G_{wz}(0, z_{rN}; h_N) \end{bmatrix}, \tag{20}$$

$$\mathbf{W}_0 = \begin{bmatrix} w_0(x_{r1}, z_{r1}) & w_0(x_{r2}, z_{r2}) & \cdots & w_0(x_{rN}, z_{rN}) \end{bmatrix}^T. \tag{21}$$

Once the resonator force amplitudes for a given incident wave field are calculated by using Eq. (D.4), the total wave field can be obtained via Eqs. (17).

4. Applications in railway-induced vibration mitigation

In this section, we exploit and validate the proposed formulation on two examples for which we also discuss the wave mitigation capabilities of the meta-trench. In particular, we first consider the surface railway scenario, by placing the wave source atop the half-space, and as a second case the subway scenario where the wave source is down in the soil. The formulation is used to compute the amplitude ratio, which measures the mitigation performance of the meta-trench over frequency, and the full wavefield. In parallel, we use full-scale FE simulations to discuss the results and validate the formulation. The mechanical and geometric parameters of the considered cases are collected in Table 1. The magnitude of the source Q_{z0} and its footprint width a are taken from common urban rail transit systems, while the meta-trench is designed with regular engineering materials (see Appendix A for details).

Table 1: Mechanical and geometric parameters for the wave source, resonators and the elastic half-space.

Symbol	Definition	Value
Q_{z0}	source amplitude in z-direction	130 kN
a	footprint length of the source	2.5 m
b	footprint length of the resonator	1.5 m
h_r	height of resonator holder	1.5 m
f_r	resonant frequency	10 Hz
m_r	mass of resonator	2675 kg
ξ_r	damping ratio of resonator	0.05
ρ	mass density of half-space	1650 kg/m^3
c_p	compressional wave velocity	427 m/s
c_s	shear wave velocity	246 m/s
ξ	hysteretic damping ratio	0.01

4.1. Surface railway scenario

For the surface railway case a harmonic load with amplitude Q_{z0} and footprint length a is applied at the surface ($x_0 = z_0 = 0$ m) of the half-space. We consider a meta-trench formed by four identical resonant units, each having width b and height h_r. The four resonators are placed at $x_r = x_0 + 8$ m and $z_r = \{-1.5, -3.0, -4.5, -6.0\}$ m, respectively. We evaluate the wave reduction capability of the meta-trench in the typical frequency range of railway-induced vibrations, i.e. 0-60 Hz. In particular, we compute the amplitude ratio A_R:

$$A_R = \left| \frac{w}{w_0} \right|. \tag{22}$$

as the ratio between the vertical displacement with and without the meta-trench, w and w_0, respectively, in a point located at the free surface at a distance $d = 10$ m behind the meta-trench, i.e. at position $x = 18$ m and $z = 0$ m. The analytical solution computed by Eq. (17b) is shown in Fig. 4a as a solid blue line.

As expected, we do observe a drop near the barrier's resonance $f_r = 10$ Hz, which suggests that a good vibration mitigation effect ($A_R < 1$) is achieved. To verify our formulation, we provide in red dashed line in Fig. 4a the solution of FE simulations obtained by using two-dimensional plane strain model (see Appendix B for details). It can be seen that the analytical solution is in very good agreement with the FE solution in the low-frequency region, as highlighted in the inset of Fig. 4b where the amplitude ratio is shown in the frequency range $[0, 15]$ Hz. Above this frequency regime a significant difference between the analytically and numerically (FE) computed A_R is observed. This discrepancy is due to the geometric scattering of the meta-trench captured

by the FE-simulated resonant units, which play a role at high frequencies, and that cannot be captured by our analytical formulation. To further prove this point, we compute through FE simulations the A_R for the classical open trench, by removing the resonators, and show the result in Fig. 4a with black dots. As can be seen the red dashed line and the black dotted line well match above 15 Hz where the attenuation is due to scattering only. The black dotted line also proves that the geometrical scattering mechanism, which requires a spatial scale of the trench comparable to the wave wavelength, the vibration mitigation in the low-frequency regime is small as $A_R \backsimeq 1$. Comparing the three lines in Fig. 4a, we conclude that the meta-trench, thanks to the resonators, has a superior vibration mitigation performance at low frequencies and that the proposed formulation can properly capture meta-trench behavior in the low-frequency range where the resonators scattered wavefields dominate the response.

In addition, we compare the total wavefield, in the region highlighted by the green dashed box ($x \in [x_r - 0.25\lambda_r, x_r + \lambda_r], y \in [0, -\lambda_r]$) in Fig. 4b, computed by our formulation and by the FE model at $f = f_r$, a frequency value for which the geometric scattering of the meta-trench plays a minor role. In the plots λ_r is the Rayleigh wavelength of the half-space at f_r. It can be seen that the analytical and FE wavefields at $f = f_r$, shown in Fig. 4c-d respectively, are in excellent agreement.

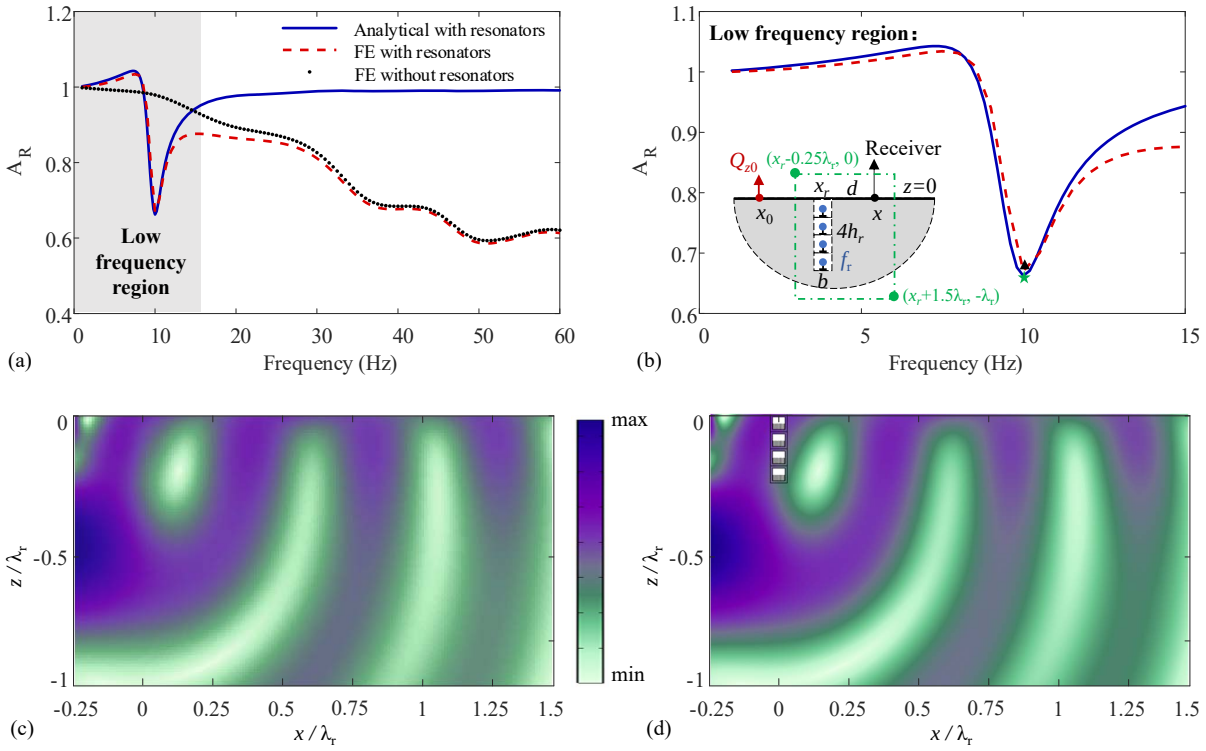

Fig. 4. Surface railway scenario. (a) Amplitude ratio: analytical solution (solid blue line) vs FE solution (red dashed line). (b) Inset of the amplitude ratio in the low-frequency region. (c) Analytical and (d) FE wavefields computed at f_r, corresponding to the points marked with a star and a triangle in Fig. 4b, respectively. In (a) we also provide the FE solution for the trench without resonators (dotted black line).

We further explore the performance of the meta-trench configured with four resonators having different resonant frequencies, namely $f_{r1} = 7$ Hz, $f_{r2} = 8$ Hz, $f_{r3} = 9$ Hz, and $f_{r4} = 10$ Hz. In this case we can expect to obtain an amplitude ratio with four valleys, around these resonant frequencies, thus broadening the attenuation zone. The amplitude ratio computed by our formulation and by the FE model is shown in Fig. 5a. As anticipated, they are in very good agreement in the low-frequency region (shaded area), and the four valleys indeed appear near the intrinsic resonant frequencies of the resonators, as better shown in the inset of Fig. 5b.

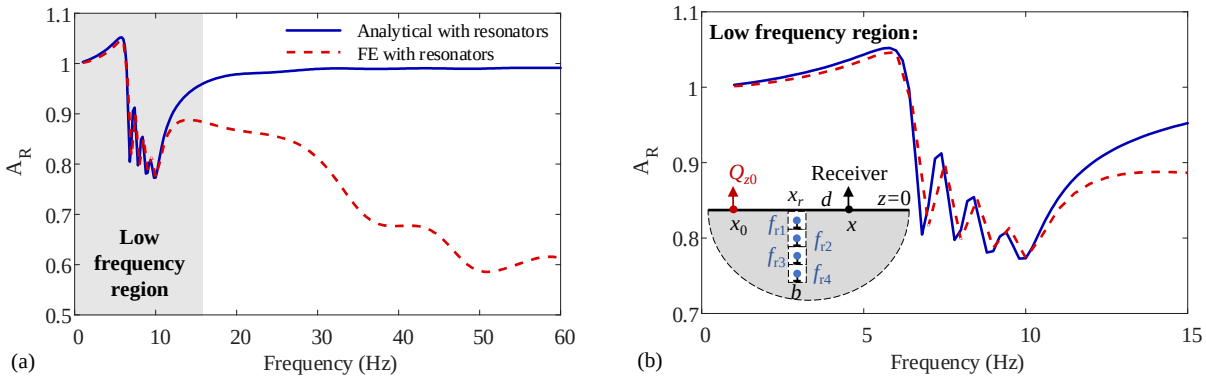

Fig. 5. Amplitude ratio for the meta-trench with four different resonators in ground railway scenario. (a)Analytical solution (solid line) vs. FE solution (dashed line); (b)Zoomed-in graph in the low-frequency region.

Comparing Fig. 5b and Fig. 4b, we can see that the effective frequency band where $A_R < 1$ is broadened in the latter scenario, which is appealing for future engineering applications.

We conclude here that the proposed formulation can be used to properly model the harmonic response of meta-trenches in the low-frequency region. Although their behavior can be simulated via commercially available FE software, the analytical formulation (i) is characterized by lower computational cost as large-scale models and numerous discrete elements are required in FE environment, and (ii) allows us to gain a deeper understanding of wave interaction problems.

4.2. Subway scenario

Let us now turn our attention to the buried-source problem and show the capability of our formulation in modeling meta-trenches for subway-induced vibrations mitigation. The subway load is simulated by a buried harmonic force applied at $x_0 = 0$ m and $z_0 = -12$ m. The force has the same amplitude and width as the first scenario. In this case, the buried exciting source generates both bulk wave and Rayleigh wave. A meta-trench having the same geometrical and mechanical parameters as the one used in Section 4.1 is located at $x_r = x_0 + 10$ m.

Proceeding in a similar way, we first consider a meta-trench with four identical resonators having resonant frequency $f_r = 10$ Hz. The analytical (blue solid line) and FE (red dashed line) computed A_R are shown in Fig. 6a in the range of $[0, 60]$ Hz. It can be seen that good agreement is found in the low-frequency range. It is worth mentioning here that a tunnel with outer radius $R = 3$ m and inner radius $r = 2.7$ m is considered in FE solution (see the detailed model in Appendix B). In the FE solution we notice that the amplitude ratio is amplified in the range of [23, 38] Hz (with $A_R > 1$) and significantly reduced in the range of [46, 60] Hz, which can be explained by geometric scattering of the meta-trench. In these frequencies, in fact, the wavelength in half space is no longer much larger than the size of trench and the geometric scattering takes place. Here, we compute the A_R for the classical open trench and plot the result with black dots in Fig. 6a. As expected, the red dashed line and the black dotted line well match above 15 Hz, which confirms that the amplification of A_R around the [23, 38] Hz range is due to geometric scattering.

In the low-frequency region, see the inset in Fig. 6b, the analytical solution matches well with the FE solution below 8 Hz, while the two solutions exhibit the same trend but different values above such frequency. When the frequency exceeds 8 Hz, in fact, the wavelength λ is less than 30 m and the geometric scattering of the tunnel cannot be ignored. However, the found discrepancy in the A_R does not weaken the potential of the

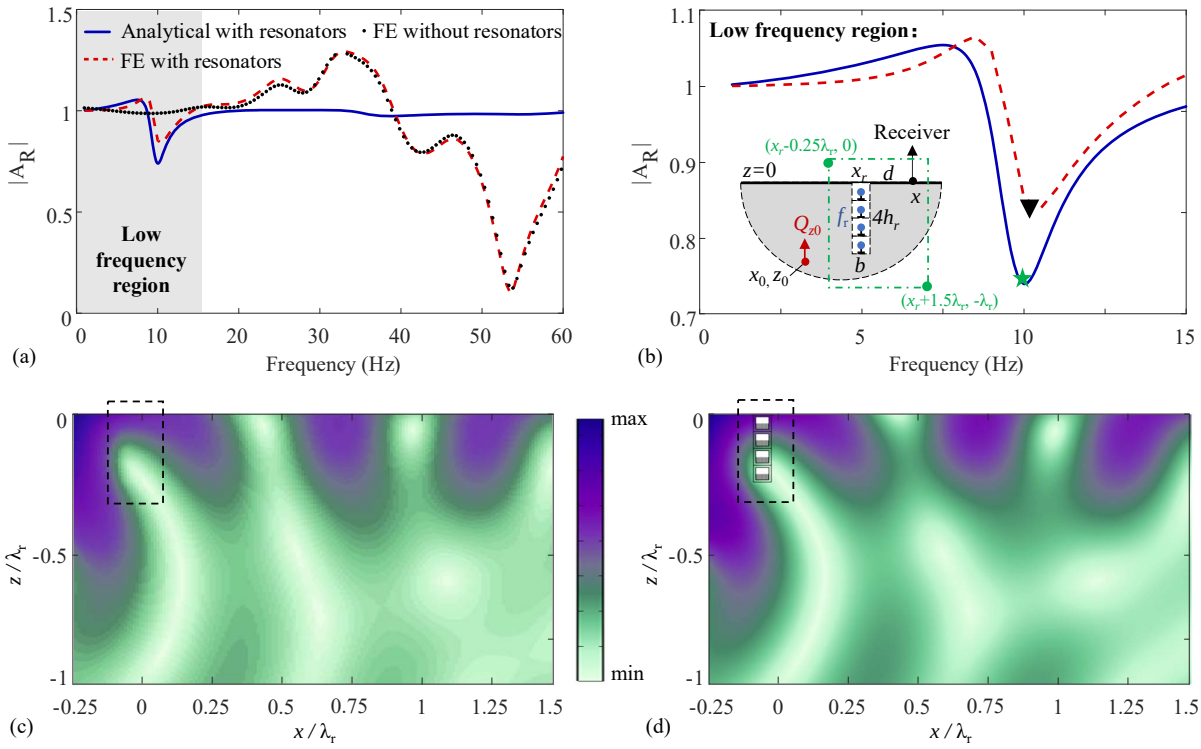

Fig. 6. Amplitude ratio for the meta-trench with four identical resonators in subway scenario (a)Analytical solution (solid line) vs. FE solution (dashed line) (b)Zoomed-in graph in the low-frequency region; (c)Analytical solution and(d) FE solution of the total wavefield at f_r, corresponding to the points marked with star and triangle in Fig. 6b respectively.

proposed formulation to unveil the dynamic of the meta-trench. This is also proven in Appendix C, where a perfect match between analytical vs FE results is found for a meta-trench having resonators with $f_r = 8$ Hz.

The total wavefield, computed by Eqs. 17 at $f = f_r$, is shown in Fig. 6c in the domain $x \in [x_r - 0.25\lambda_r, x_r + 1.5\lambda_r]$, $z \in [-\lambda_r, 0]$, i.e., the green dashed region highlighted in Fig. 6b. From a global perspective, the analytical wavefield is in good agreement with the one displayed in Fig. 6d, which is obtained from the FE solution. Furthermore, no discrepancies caused by geometric scattering are observed in the area adjacent to the meta-trench (the black dashed region in Fig. 6c-d), confirming the validity of the proposed formulation to model the meta-trench for subway-induced vibrations.

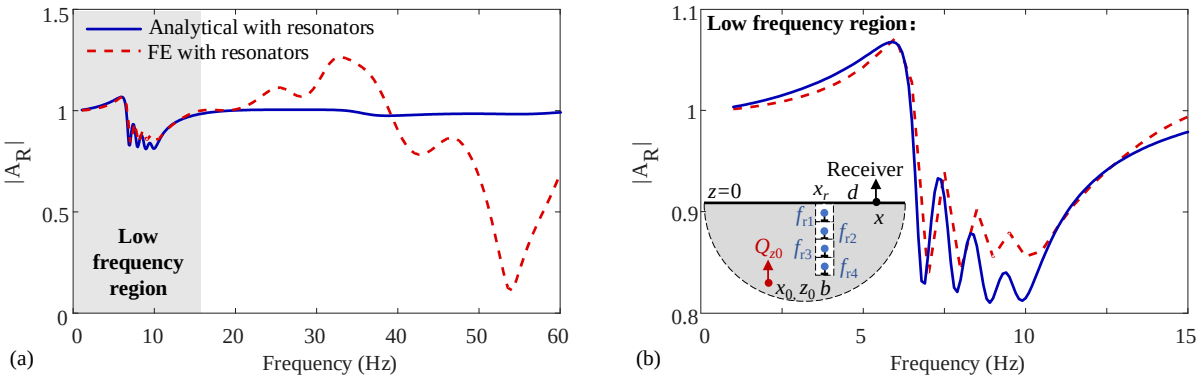

Fig. 7. Amplitude ratio for the meta-trench with four different resonators in the subway scenario. (a) Analytical solution (solid line) vs. FE solution (dashed line); (b) Inset in the low-frequency region.

Next, we consider the meta-trench with resonators having resonant frequencies of $\{7, 8, 9, 10\}$ Hz, and compute the amplitude ratio A_R. The results are shown in Fig. 7a and 7b. We observe similarities with the case

shown in Fig. 5: a perfect match between the analytical and the FE solutions in the low-frequency region, multiple drops near the resonant frequencies of the resonators, and a broaden frequency range with $A_R < 1$ compared to the case with identical resonators. Finally, we remark that the computation of the amplitude ratio in the above figures using our analytical approach takes only a few seconds. In contrast, the finite element (FE) approach necessitates the use of two separate FE models (i.e., one for the free field computation and another for the total field calculation) and a computational time of tens of minutes.

5. Conclusion

We have developed a multiple scattering formulation to compute the wave-coupled response of a cluster of resonators (known as a meta-trench) distributed into an isotropic half-space. The formulation allows one to consider an incident wave field generated both atop and inside the half-space. The incident and scattered wave fields, the latter generated by the motion of the resonators, are described via ad-hoc formulated Green's functions where the amplitudes of the scattered wave fields are obtained from the multiple scattering formulation imposing proper boundary conditions.

The proposed formulation has been used to model different meta-trenches and assess their wave mitigation capabilities for both ground railway and subway induced vibrations. A validation case carried out via finite element simulations has proved that the formulation properly captures the dynamic of meta-trenches in the low-frequency regime where the geometric scattering of the resonant units can be neglected. In this low-frequency range, the meta-trenches, thanks to their resonant scattering mechanism, exceed classic in-filled trench barriers in mitigating vibrations.

It must be remarked here that aside meta-trenches the proposed formulation permits to model the coupled response of an array of resonators with no limitation on their number nor on their position. As such the formulation can serve different metamaterials-related research. We envision that our formulation can be extended to design novel devices for seismic wave manipulation, wave localization and energy harvesting.

CRediT authorship contribution statement

Kemeng Cui: Conceptualization, Methodology, Investigation, Software, Writing - original draft. **Xingbo Pu:** Conceptualization, Methodology, Validation, Writing - review & editing, Supervision. **Alessandro Marzani:** Conceptualization, Investigation, Writing - review & editing, Supervision. **Zhao-dong Xu:** Conceptualization, Writing - review & editing, Supervision, Funding acquisition.

Declaration of competing interest

The authors declare that they have no conflict of interest.

Acknowledgments

This project has received funding from the Major Project of Fundamental Research on Frontier Leading Technology of Jiangsu Province (NO.BK20222006), National Natural Science Foundation of China (52130807), National Key Research and Development Plans (No.2019YFE0121900), the Anhui Province Key Research and Development Plans (202104G01020002), the Tencent Foundation through the XPLORER PRIZE, and the program of

China Scholarships Council (202006090272). X.P. acknowledges the support of the European Union's Horizon 2020 research and innovation programme under the Marie Skłodowska Curie grant agreement No 813424.

Appendix A. Structural and material parameters of the meta-trench

In this appendix, we provide the design strategy and parameters of the proposed meta-trench. In practice, the meta-trench is embedded in a three-dimensional (3D) half-space as shown in Fig. A.1a. We design a 3D unit of meta-trench with dimensions $b_1 \times b_1 \times h_1$ as per Fig. A.1b, and the sectional view is shown in Fig. A.1c. The unit has three components: a concrete box ($1^{\#}$) as the holder with thickness $t = 0.2$ m, a stiff inner core ($2^{\#}$) and its flexible supports ($3^{\#}$). Typically, the inner core is made of engineered steel with high density, which acts as a mass element. By contrast, the flexible supports acting as springs are required to be elastic and lightweight, whose favorable material can be rubber. In this paper, the flexible supports are made of the widely used nitrile butadiene rubber (NBR) [40, 41]. The material and geometrical parameters used in our meta-trench are listed in Table A.1.

The vibration mitigation performance of meta-trench originates from the mechanism of local resonance, where the inner steel core plays the mass $m = \rho_2 \cdot {b_2}^2 \cdot h_2 = 2675$ kg, and the rubber blocks act as springs with a total stiffness $k = 2E_3 \cdot {b_3}^2/h_3 = 10500$ kN/m. These designed parameters yield the desired resonant frequency $f = \frac{1}{2\pi}\sqrt{k/m} = 10$ Hz in Table 1. We keep the stiffness constant and adjust the mass, essentially the size b_2, to obtain different resonant frequencies. Assuming the out-of-plane (along y) invariance of the configuration, we investigate the problem via the two-dimensional plane model (Fig. A.1d). Such a 2D model is used for the FE simulation in Appendix B.

We remark here that as discussed in some recent works the resonator mass could be reduced, reducing thus the meta-trench costs, by leveraging inertial amplification mechanisms [42, 43].

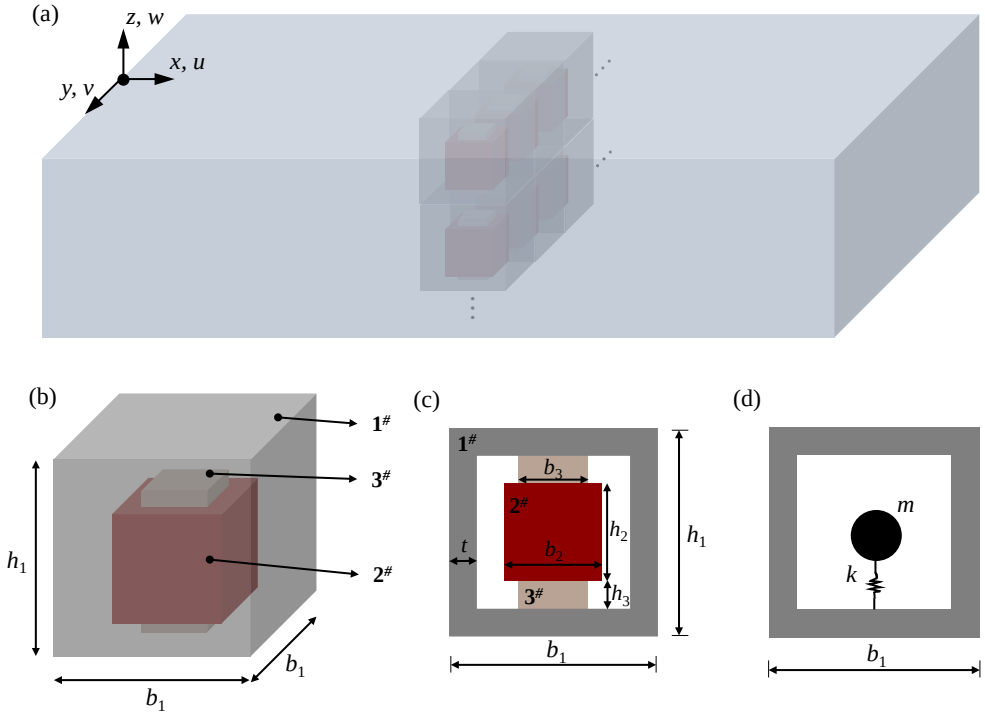

Fig. A.1. Unit cell of the meta-trench (a) Arrangement scheme in a 3D half-space. (b) 3D structure. (c) Sectional view of the unit cell. (d) Equivalent 2D model.

Table A.1: Material and geometrical parameters of meta-trench.

Symbol	Material	Young's modulus E_i	Density ρ_i	Poisson's ratio ν_i	Width b_i	Height h_i
$1^{\#}$	Concrete (C30)	30 GPa	2500 kg/m^3	0.3	1.5 m	1.5 m
$2^{\#}$	Steel	210 GPa	7800 kg/m^3	0.3	0.7 m	0.7 m
$3^{\#}$	Rubber (NBR)	4.2 MPa	1200 kg/m^3	0.49	0.5 m	0.2 m

Appendix B. Detailed FE models

Here we provide the FE models used to validate our formulation in Section 4. The two-dimensional half-space is modeled in COMSOL Multiphysics by a finite-size area with absorbing boundary conditions (Perfectly Matched Layers) as in Fig. B.1. As mentioned in Section 4, the meta-trench embedded in the half-space is composed of four resonant units, each of them encasing one resonator. To simulate the uniform vertical dynamic force over the footprint area b, each resonator is modeled by means of ten truss massless elements with concentrated masses $\bar{m} = m/10$ atop; the Young modulus of the truss is $E_t = (\bar{m}\omega_r^2 + \mathrm{i}\omega c)l_t/A_t$, where l_t and A_t are the length and the cross-section area of the truss. The distances source-trench and source-receiver are identical to those considered in Section 4. In our analysis, we ensure consistency between the finite element (FE) models and the analytical formulation by employing the same damping ratio ξ. This is accomplished by specifying the complex moduli of the soil material within the FE models as $\lambda(1 + 2\xi\mathrm{i})$ and $\mu(1 + 2\xi\mathrm{i})$.

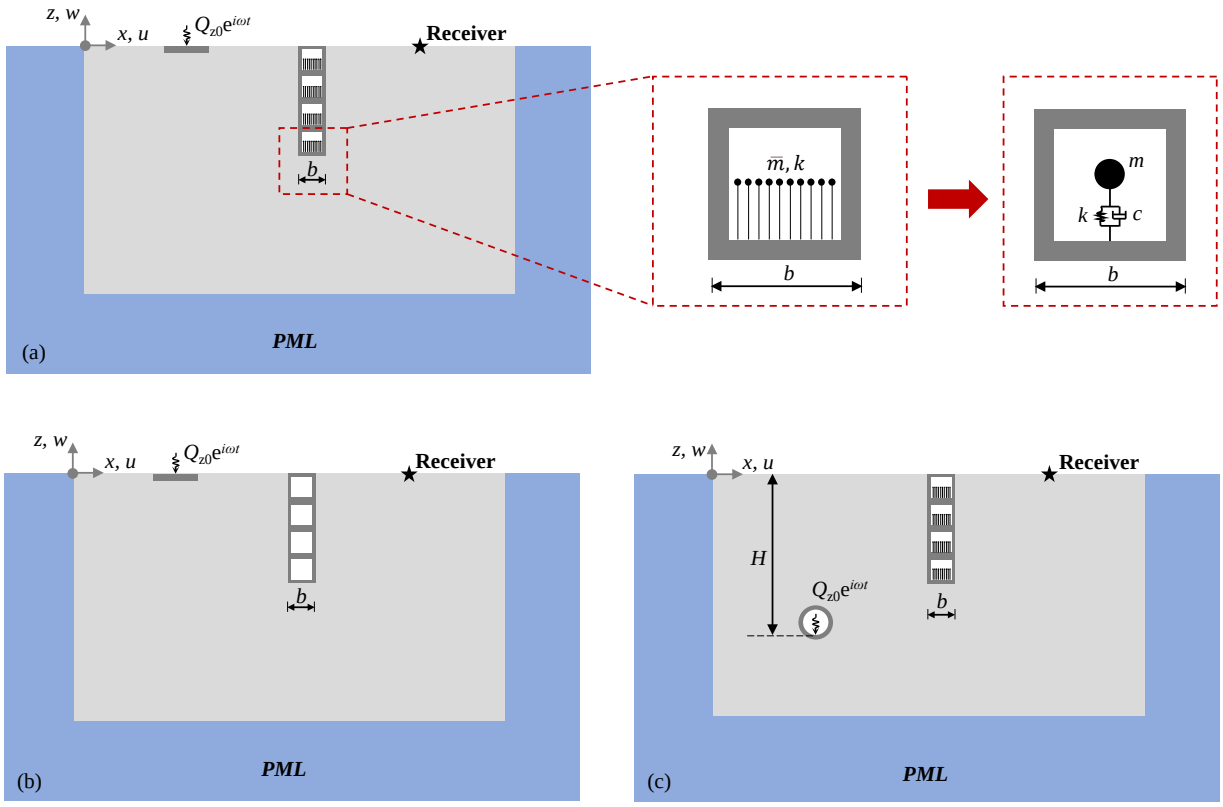

Fig. B.1. Schematic of the FE models used for the surface railway scenario with resonators and without resonators in (a) and (b), respectively. (c) FE model used for subway scenario

.

The FE models used for the various cases discussed in Section 4 are shown in Fig. B.1a, Fig. B.1b and Fig. B.1c. For the cases in Fig. B.1a-c the source $Q_{z0}e^{\mathrm{i}\omega t}$ is located at the free surface over a footprint width a. The case in Fig. B.1b has been used to model the classical trench with no resonators to study the geometric

scattering effect only. Fig. B.1c shows the FE model used for the subway scenario where the source is located inside the tunnel at a depth of $H = 10$ m.

Appendix C. Subway scenario: $f_r = 8$ Hz

All the geometrical and mechanical parameters considered here are identical to those used in Section 4.2, except for the resonators resonant frequency $f_r = 8$ Hz. In this case, the wavelength at the resonant frequency is $\lambda_r = 30$ m, i.e., five times the tunnel size. As such the geometric scattering due to the presence of the tunnel can be omitted.

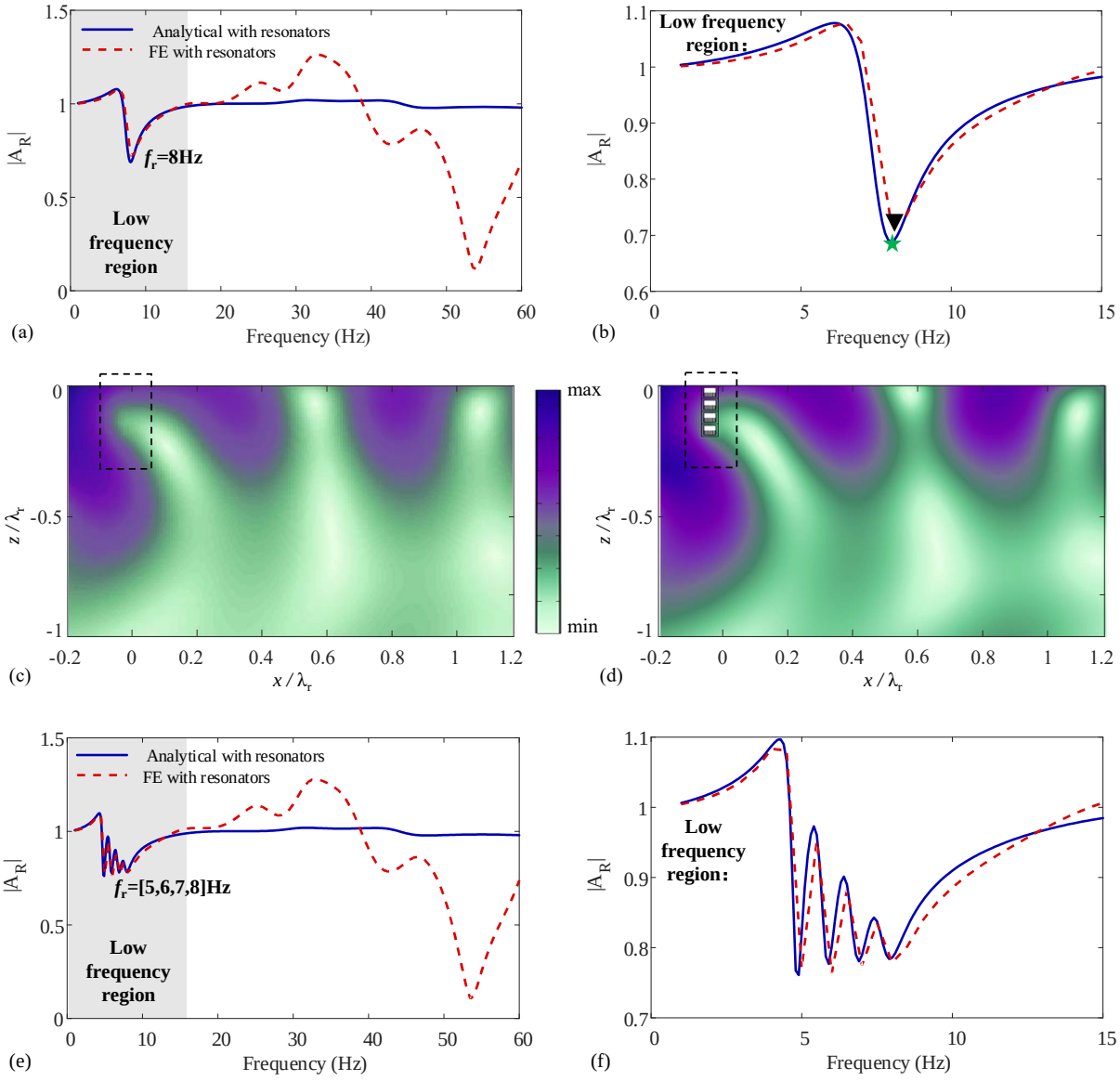

Fig. C.2. (a) analytical (solid line) vs. FE (red dashed line) amplitude ratio for the meta-trench with identical resonators ($f_r = 8$ Hz) for the subway scenario. (b) Inset in the low-frequency region. (c) analytical and (d) FE total wavefield at $f_r = 8$ Hz (computed at the points marked with star and triangle in Fig. C.2b respectively). Amplitude ratio (e) analytical (blue solid line) vs FE (red dashed line) solution for the meta-trench with different resonators. (f) Inset in the low-frequency region.

Proceeding as in Section 4.2, we calculate the A_R by using the proposed formulation and the FE models. The amplitude ratio and the total wavefields at $f_r = 8$ Hz are shown in Fig. C.2. It can be clearly seen that the analytical amplitude ratio A_R perfectly matches in low-frequency region, and in this case also the resonant

frequency of resonators are in very good agreement (Fig. C.2a-b and Fig. C.2e-f). Also the analytical wavefield in Fig. C.2c is in excellent agreement with the one in Fig. C.2d obtained from the FE model.

Despite the fact that the tunnel exists in a practical subway scenario, our formulation still accurately captures the amplitude ratio in low-frequency range. Thus, the engineering applicability of our formulation is confirmed by this Appendix.

Appendix D. Extended formulation for a resonator with two degrees of freedom

In order to account for both the vertical and horizontal degrees of freedom, the resonator is modeled using a mass and two springs, as illustrated in Fig. D.1. By following the same derivation procedure outlined in Section 3, we obtain the vertical and horizontal force amplitudes, denoted as Q_{nx} and Q_{nz}, respectively, for the nth resonator. These force amplitudes are obtained from the dynamic equilibrium equations:

$$Q_{nx} = Z_{nx}u(x_{rn}, z_{rn}) = \frac{m_n\omega^2(\mathrm{i}\omega c_{nx} + m_n{\omega_{rnx}}^2)}{-m_n\omega^2 + \mathrm{i}\omega c_{nx} + m_n{\omega_{rnx}}^2}u(x_{rn}, z_{rn}) \quad n = 1, ..., N, \tag{D.1a}$$

$$Q_{nz} = Z_{nz}w(x_{rn}, z_{rn}) = \frac{m_n\omega^2(\mathrm{i}\omega c_{nz} + m_n{\omega_{rnz}}^2)}{-m_n\omega^2 + \mathrm{i}\omega c_{nz} + m_n{\omega_{rnz}}^2}w(x_{rn}, z_{rn}) \quad n = 1, ..., N, \tag{D.1b}$$

with $\omega_{rnx} = 2\pi f_{rnx} = \sqrt{k_{nx}/m_n}$, $\omega_{rnz} = 2\pi f_{rnz} = \sqrt{k_{nz}/m_n}$, in which m_n is the mass of the nth resonator, k_{nx} and k_{nz} are the stiffnesses of the horizontal and vertical springs respectively, c_{nx} and c_{nz} are the damping coefficients of the horizontal vertical springs, respectively.

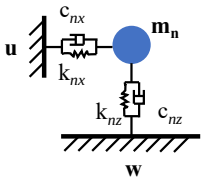

Fig. D.1. Resonator with two degrees of freedom.

Then, the total wavefield in Eqs. (17) are replaced by:

$$u(x, z) = u_0(x, z) + \sum_{n=1}^{N} Q_{nx}G_{ux}(x - x_{rn}, z; h_{rn}) + \sum_{n=1}^{N} Q_{nz}G_{uz}(x - x_{rn}, z; h_{rn}) \tag{D.2a}$$

$$w(x, z) = w_0(x, z) + \sum_{n=1}^{N} Q_{nx}G_{wx}(x - x_{rn}, z; h_{rn}) + \sum_{n=1}^{N} Q_{nz}G_{wz}(x - x_{rn}, z; h_{rn}) \tag{D.2b}$$

Accordingly, the displacements at the base of the jth resonator in Eq. (18) is rewritten as:

$$Z_{jx}^{-1}Q_{jx} = u_0(x_{rj}, z_{rj}) + \sum_{n=1}^{N} Q_{nx}G_{ux}(x_{rj} - x_{rn}, z_{rj}; h_{rn}) + \sum_{n=1}^{N} Q_{nz}G_{uz}(x_{rj} - x_{rn}, z_{rj}; h_{rn}) \tag{D.3a}$$

$$Z_{jz}^{-1}Q_{jz} = w_0(x_{rj}, z_{rj}) + \sum_{n=1}^{N} Q_{nx}G_{wx}(x_{rj} - x_{rn}, z_{rj}; h_{rn}) + \sum_{n=1}^{N} Q_{nz}G_{wz}(x_{rj} - x_{rn}, z_{rj}; h_{rn}) \tag{D.3b}$$

The matrix form of Eqs. (D.3) is similar to Eq. (D.4):

$$\mathbf{Q} = \mathbf{A}^{-1}\mathbf{D_0} \tag{D.4}$$

where $\mathbf{Q} = [\mathbf{Q_x}, \mathbf{Q_z}]^T$ is the vector of the sought resonator force amplitudes, with horizontal force $\mathbf{Q_x} = [Q_{1x}, Q_{2x}, \cdots, Q_{Nx}]^T$ and vertical force $\mathbf{Q_z} = [Q_{1z}, Q_{2z}, \cdots, Q_{Nz}]^T$. It should be noted that the size of $\mathbf{A}$ and $\mathbf{D_0}$ here turn to $2N \times 2N$ and $2N \times 1$, respectively:

$$\mathbf{A} = \begin{bmatrix} \mathbf{A_{11}} & \mathbf{A_{12}} \\ \mathbf{A_{21}} & \mathbf{A_{22}} \end{bmatrix}, \ \mathbf{D_0} = [\mathbf{U_0}, \mathbf{W_0}]^T \tag{D.5}$$

with

$$\mathbf{A_{11}} = \begin{bmatrix} Z_{1x}^{-1} - G_{ux}(0, z_{r1}; h_1) & -G_{ux}(x_{r1} - x_{r2}, z_{r1}; h_2) & \cdots & -G_{ux}(x_{r1} - x_{rN}, z_{r1}; h_N) \\ -G_{ux}(x_{r2} - x_{r1}, z_{r2}; h_1) & Z_{2x}^{-1} - G_{ux}(0, z_{r2}; h_2) & \cdots & -G_{ux}(x_{r2} - x_{rN}, z_{r2}; h_N) \\ \vdots & \vdots & \ddots & \vdots \\ -G_{ux}(x_{rN} - x_{r1}, z_{rN}; h_1) & -G_{ux}(x_{rN} - x_{r2}, z_{rN}; h_2) & \cdots & Z_{Nx}^{-1} - G_{ux}(0, z_{rN}; h_N) \end{bmatrix}, \tag{D.6a}$$

$$\mathbf{A_{12}} = \begin{bmatrix} -G_{uz}(0, z_{r1}; h_1) & -G_{uz}(x_{r1} - x_{r2}, z_{r1}; h_2) & \cdots & -G_{uz}(x_{r1} - x_{rN}, z_{r1}; h_N) \\ -G_{uz}(x_{r2} - x_{r1}, z_{r2}; h_1) & -G_{uz}(0, z_{r2}; h_2) & \cdots & -G_{uz}(x_{r2} - x_{rN}, z_{r2}; h_N) \\ \vdots & \vdots & \ddots & \vdots \\ -G_{uz}(x_{rN} - x_{r1}, z_{rN}; h_1) & -G_{uz}(x_{rN} - x_{r2}, z_{rN}; h_2) & \cdots & -G_{uz}(0, z_{rN}; h_N) \end{bmatrix}, \tag{D.6b}$$

$$\mathbf{A_{21}} = \begin{bmatrix} -G_{wx}(0, z_{r1}; h_1) & -G_{wx}(x_{r1} - x_{r2}, z_{r1}; h_2) & \cdots & -G_{wx}(x_{r1} - x_{rN}, z_{r1}; h_N) \\ -G_{wx}(x_{r2} - x_{r1}, z_{r2}; h_1) & -G_{wx}(0, z_{r2}; h_2) & \cdots & -G_{wx}(x_{r2} - x_{rN}, z_{r2}; h_N) \\ \vdots & \vdots & \ddots & \vdots \\ -G_{wx}(x_{rN} - x_{r1}, z_{rN}; h_1) & -G_{wx}(x_{rN} - x_{r2}, z_{rN}; h_2) & \cdots & -G_{wx}(0, z_{rN}; h_N) \end{bmatrix}, \tag{D.6c}$$

$$\mathbf{A_{22}} = \begin{bmatrix} Z_{1z}^{-1} - G_{wz}(0, z_{r1}; h_1) & -G_{wz}(x_{r1} - x_{r2}, z_{r1}; h_2) & \cdots & -G_{wz}(x_{r1} - x_{rN}, z_{r1}; h_N) \\ -G_{wz}(x_{r2} - x_{r1}, z_{r2}; h_1) & Z_{2z}^{-1} - G_{wz}(0, z_{r2}; h_2) & \cdots & -G_{wz}(x_{r2} - x_{rN}, z_{r2}; h_N) \\ \vdots & \vdots & \ddots & \vdots \\ -G_{wz}(x_{rN} - x_{r1}, z_{rN}; h_1) & -G_{wz}(x_{rN} - x_{r2}, z_{rN}; h_2) & \cdots & Z_{Nz}^{-1} - G_{wz}(0, z_{rN}; h_N) \end{bmatrix}, \tag{D.6d}$$

$$\mathbf{U}_0 = \begin{bmatrix} u_0(x_{r1}, z_{r1}) & u_0(x_{r2}, z_{r2}) & \cdots & u_0(x_{rN}, z_{rN}) \end{bmatrix}. \tag{D.7a}$$

$$\mathbf{W}_0 = \begin{bmatrix} w_0(x_{r1}, z_{r1}) & w_0(x_{r2}, z_{r2}) & \cdots & w_0(x_{rN}, z_{rN}) \end{bmatrix}. \tag{D.7b}$$

The Green's functions G_{uz} and G_{wz} are already given by Eqs. (11), and we would supplement here the functions of G_{ux} and G_{wx}:

$$\mathbf{G}'(x, z; h) = \frac{1}{2\pi\mu a} \int_{-\infty}^{\infty} \frac{1}{{k_s}^2 \gamma_1} \mathbf{\Delta}' \mathbf{Y} \sin\frac{ka}{2} \mathrm{e}^{\mathrm{i}kx} \, \mathrm{d}k, \tag{D.8}$$

where $\mathbf{G}'(x,z;h)=[G_{ux},G_{wx}]^T$, $\mathbf{Y}=[\mathrm{e}^{pz},\mathrm{e}^{-pz},\mathrm{e}^{qz},\mathrm{e}^{-qz}]^T$, and $\mathbf{\Delta}'$ is equal to:

$$\mathbf{\Delta}'=\begin{bmatrix} \frac{k}{p}(\mathrm{e}^{hp}\gamma_2+4\mathrm{e}^{hq}pq\beta) & \frac{k}{p}\mathrm{e}^{hp}\gamma_1 & \frac{q}{k}(4\mathrm{e}^{hp}k^2\beta+\mathrm{e}^{hq}\gamma_2) & -\frac{q}{k}\mathrm{e}^{hq}\gamma_1 \\ -\mathrm{i}(\mathrm{e}^{hp}\gamma_2+4\mathrm{e}^{hq}pq\beta) & \mathrm{i}\mathrm{e}^{hp}\gamma_1 & -\mathrm{i}(4\mathrm{e}^{hp}k^2\beta+\mathrm{e}^{hq}\gamma_2) & -\mathrm{i}\mathrm{e}^{hq}\gamma_1 \end{bmatrix} \tag{D.9}$$

if $z>h$ and equals to the following item if $z\leq h$:

$$\mathbf{\Delta}'=\begin{bmatrix} \frac{k}{p}(\mathrm{e}^{hp}\gamma_2+\mathrm{e}^{-hp}\gamma_1+4\mathrm{e}^{hq}pq\beta) & 0 & \frac{q}{k}(4\mathrm{e}^{hp}k^2\beta+\mathrm{e}^{hq}\gamma_2-\mathrm{e}^{-hq}\gamma_1) & 0 \\ -\mathrm{i}(\mathrm{e}^{hp}\gamma_2+\mathrm{e}^{-hp}\gamma_1+4\mathrm{e}^{hq}pq\beta) & 0 & -\mathrm{i}(4\mathrm{e}^{hp}k^2\beta+\mathrm{e}^{hq}\gamma_2-\mathrm{e}^{-hq}\gamma_1) & 0 \end{bmatrix} \tag{D.10}$$

References

[1] D. Clouteau, G. Degrande, G. Lombaert, Numerical modelling of traffic induced vibrations, Meccanica 36 (4) (2001) 401–420. doi:10.1023/A:1015005410628.

[2] K. Kuo, M. Papadopoulos, G. Lombaert, G. Degrande, The coupling loss of a building subject to railway induced vibrations: Numerical modelling and experimental measurements, J. Sound Vib. 442 (2019) 459–481. doi:10.1016/j.jsv.2018.10.048.

[3] D. Beskos, B. Dasgupta, I. Vardoulakis, Vibration isolation using open or filled trenches, Comput Mech 1 (1) (1986) 43–63. doi:10.1007/BF00298637.

[4] Y.-B. Yang, H.-H. Hung, Wave propagation for train-induced vibrations: a finite/infinite element approach, World Scientific, 2009. doi:10.1142/7062.

[5] D. Thompson, J. Jiang, M. Toward, M. Hussein, E. Ntotsios, A. Dijckmans, P. Coulier, G. Lombaert, G. Degrande, Reducing railway-induced ground-borne vibration by using open trenches and soft-filled barriers, Soil Dyn. Earthq. Eng. 88 (2016) 45–59. doi:10.1016/j.soildyn.2016.05.009.

[6] J. B. Li, Z. W. Hu, Z. D. Xu, Y. Q. Guo, Three-dimensional dynamic analysis of ancient buildings with novel high damping isolation trenches, J. Vib. Control 28 (17-18) (2022) 2409–2420. doi:10.1177/10775463211010910.

[7] S. Kattis, D. Polyzos, D. Beskos, Modelling of pile wave barriers by effective trenches and their screening effectiveness, Soil Dyn. Earthq. Eng. 18 (1) (1999) 1–10. doi:10.1016/S0267-7261(98)00032-3.

[8] J. Huang, Z. Shi, Application of periodic theory to rows of piles for horizontal vibration attenuation, Int. J. Geomech 10 (1061) (2013) 132–142. doi:10.1061/(ASCE)GM.1943-5622.0000193.

[9] L. Meng, Z. Cheng, Z. Shi, Vibration mitigation in saturated soil by periodic pile barriers, Comput Geotech 117 (2020) 103251. doi:10.1016/j.compgeo.2019.103251.

[10] C. He, S. Zhou, P. Guo, Mitigation of railway-induced vibrations by using periodic wave impeding barriers, Appl. Math. Model. 105 (2022) 496–513. doi:10.1016/j.apm.2021.12.053.

[11] Z. Liu, X. Zhang, Y. Mao, Y. Zhu, Z. Yang, C. T. Chan, P. Sheng, Locally resonant sonic materials, Science 289 (5485) (2000) 1734–1736. doi:10.1126/science.289.5485.1734.

[12] X. Zhou, X. Liu, G. Hu, Elastic metamaterials with local resonances: an overview, Theor. App. Mech. Lett. 2 (4) (2012) 041001. doi:10.1063/2.1204101.

[13] D. Bigoni, S. Guenneau, A. B. Movchan, M. Brun, Elastic metamaterials with inertial locally resonant structures: Application to lensing and localization, Phys. Rev. B 87 (17) (2013) 174303. doi:10.1103/PhysRevB.87.174303.

[14] A. Colombi, P. Roux, S. Guenneau, M. Rupin, Directional cloaking of flexural waves in a plate with a locally resonant metamaterial, J. Acoust. Soc. Am. 137 (4) (2015) 1783–1789. doi:10.1121/1.4915004.

[15] W. Zhou, Z. Sun, S. Wu, Z. Fan, Compact and efficient elastic metasurface based on mass-stiffness relation for manipulation of flexural waves, J. Sound Vib. 541 (2022) 117291. doi:10.1016/j.jsv.2022.117291.

[16] C. Sugino, A. Erturk, Analysis of multifunctional piezoelectric metastructures for low-frequency bandgap formation and energy harvesting, J. Phys. D-Appl. Phys. 51 (21) (2018) 215103. doi:10.1088/1361-6463/aab97e.

[17] G. J. Chaplain, J. M. De Ponti, G. Aguzzi, A. Colombi, R. V. Craster, Topological rainbow trapping for elastic energy harvesting in graded su-schrieffer-heeger systems, Phys. Rev. Appl. 14 (5) (2020) 054035. doi:10.1103/PhysRevApplied.14.054035.

[18] E. Garova, A. Maradudin, A. Mayer, Interaction of rayleigh waves with randomly distributed oscillators on the surface, Phys. Rev. B 59 (20) (1999) 13291. doi:10.1103/PhysRevB.59.13291.

[19] M. Nouh, O. Aldraihem, A. Baz, Wave propagation in metamaterial plates with periodic local resonances, J. Sound Vib. 341 (2015) 53–73. doi:10.1016/j.jsv.2014.12.030.

[20] S. Brûlé, S. Enoch, S. Guenneau, Emergence of seismic metamaterials: Current state and future perspectives, Phys. Lett. A 384 (1) (2020) 126034. doi:10.1016/j.physleta.2019.126034.

[21] M. Al Lethawe, M. Addouche, S. Benchabane, V. Laude, A. Khelif, Guidance of surface elastic waves along a linear chain of pillars, AIP Adv. 6 (12) (2016) 121708. doi:10.1063/1.4972552.

[22] Muhammad, C. Lim, J. Reddy, Built-up structural steel sections as seismic metamaterials for surface wave attenuation with low frequency wide bandgap in layered soil medium, Eng. Struct. 188 (2019) 440–451. doi:10.1016/j.engstruct.2019.03.046.

[23] L. Cao, Z. Yang, Y. Xu, Z. Chen, Y. Zhu, S.-W. Fan, K. Donda, B. Vincent, B. Assouar, Pillared elastic metasurface with constructive interference for flexural wave manipulation, Mech. Syst. Signal Proc. 146 (2021) 107035. doi:10.1016/j.ymssp.2020.107035.

[24] A. Colombi, P. Roux, S. Guenneau, P. Gueguen, R. V. Craster, Forests as a natural seismic metamaterial: Rayleigh wave bandgaps induced by local resonances, Sci Rep 6 (1) (2016) 1–7. doi:10.1038/srep19238.

[25] D. Colquitt, A. Colombi, R. Craster, P. Roux, S. Guenneau, Seismic metasurfaces: Sub-wavelength resonators and rayleigh wave interaction, J. Mech. Phys. Solids 99 (2017) 379–393. doi:10.1016/j.jmps.2016.12.004.

[26] G. J. Chaplain, J. M. De Ponti, A. Colombi, R. Fuentes-Dominguez, P. Dryburg, D. Pieris, R. J. Smith, A. Clare, M. Clark, R. V. Craster, Tailored elastic surface to body wave umklapp conversion, Nat. Commun. 11 (1) (2020) 1–6. doi:10.1038/s41467-020-17021-x.

[27] A. Palermo, S. Krödel, A. Marzani, C. Daraio, Engineered metabarrier as shield from seismic surface waves, Sci Rep 6 (1) (2016) 1–10. doi:10.1038/srep39356.

[28] A. Palermo, M. Vitali, A. Marzani, Metabarriers with multi-mass locally resonating units for broad band rayleigh waves attenuation, Soil Dyn. Earthq. Eng. 113 (2018) 265–277. doi:10.1016/j.soildyn.2018.05.035.

[29] F. Zeighami, A. Palermo, A. Marzani, Rayleigh waves in locally resonant metamaterials, Int. J. Mech. Sci. 195 (2021) 106250. doi:10.1016/j.ijmecsci.2020.106250.

[30] A. Maurel, J.-J. Marigo, K. Pham, S. Guenneau, Conversion of love waves in a forest of trees, Phys. Rev. B 98 (13) (2018) 134311. doi:10.1103/PhysRevB.98.134311.

[31] J.-J. Marigo, K. Pham, A. Maurel, S. Guenneau, Effective model for elastic waves propagating in a substrate supporting a dense array of plates/beams with flexural resonances, J. Mech. Phys. Solids 143 (2020) 104029. doi:10.1016/j.jmps.2020.104029.

[32] I. A. Veres, T. Berer, Complexity of band structures: Semi-analytical finite element analysis of one-dimensional surface phononic crystals, Phys. Rev. B 86 (10) (2012) 104304. doi:10.1103/PhysRevB.86.104304.

[33] Y. Zeng, P. Peng, Q.-J. Du, Y.-S. Wang, B. Assouar, Subwavelength seismic metamaterial with an ultra-low frequency bandgap, J. Appl. Phys. 128 (1) (2020) 014901. doi:10.1063/1.5144177.

[34] X. Pu, A. Palermo, Z. Cheng, Z. Shi, A. Marzani, Seismic metasurfaces on porous layered media: Surface resonators and fluid-solid interaction effects on the propagation of rayleigh waves, Int. J. Eng. Sci. 154 (2020) 103347. doi:10.1016/j.ijengsci.2020.103347.

[35] X. Pu, A. Palermo, A. Marzani, Lamb's problem for a half-space coupled to a generic distribution of oscillators at the surface, Int. J. Eng. Sci. 168 (2021) 103547. doi:10.1016/j.ijengsci.2021.103547.

[36] X. Pu, A. Palermo, A. Marzani, Topological edge states of quasiperiodic elastic metasurfaces, Mech. Syst. Signal Proc. 181 (2022) 109478. doi:10.1016/j.ymssp.2022.109478.

[37] X. Pu, A. Palermo, A. Marzani, A multiple scattering formulation for finite-size flexural metasurfaces, Proc. R. Soc. A 478 (2262) (2022) 20210669. doi:10.1098/rspa.2021.0669.

[38] H. Howarth, M. Griffin, Human response to simulated intermittent railway-induced building vibration, J. Sound Vib. 120 (2) (1988) 413–420. doi:10.1016/0022-460X(88)90453-1.

[39] R. Pak, Asymmetric wave propagation in an elastic half-space by a method of potentials, J. Appl. Mech. 54 (1) (1987) 121–126. doi:10.1115/1.3172945.

[40] Z. D. Xu, Y. X. Liao, T. Ge, C. Xu, Experimental and theoretical study of viscoelastic dampers with different matrix rubbers, J. Eng. Mech.-ASCE 142 (8) (2016) 04016051. doi:10.1061/(ASCE)EM.1943-7889.0001101.

[41] T. Ge, Z. D. Xu, F.-G. Yuan, Development of viscoelastic damper based on NBR and organic small-molecule composites, J. Mater. Civ. Eng. 34 (8) (2022) 04022192. doi:10.1061/(ASCE)MT.1943-5533.0004339.

[42] F. Zeighami, A. Palermo, A. Marzani, Inertial amplified resonators for tunable metasurfaces, Meccanica 54 (2019) 2053–2065. doi:10.1007/s11012-019-01020-4.

[43] Y. Zeng, L. Cao, S. Wan, T. Guo, Y.-F. Wang, Q.-J. Du, B. Assouar, Y.-S. Wang, Seismic metamaterials: Generating low-frequency bandgaps induced by inertial amplification, Int. J. Mech. Sci. 221 (2022) 107224. doi:10.1016/j.ijmecsci.2022.107224.